Tunable Doping and Optoelectronic Modulation in Graphene-Covered 4H-SiC Surfaces

Masoud Mansouri,[*,†] Fernando Martín,[†,‡] and Cristina Díaz[¶]

[†]*Departamento de Química, Módulo 13, Universidad Autónoma de Madrid, Madrid, 28049, Spain*

[‡]*Instituto Madrileño de Estudios Avanzados en Nanociencia (IMDEA Nano), Campus de Cantoblanco, Madrid, 28049, Spain*

[¶]*Departamento de Química Física, Facultad de CC Químicas, Universidad Complutense de Madrid, Madrid, 28040, Spain*

E-mail: masoud.mansouri@uam.es

Abstract

Semiconducting graphene is pivotal in the advancement of nanoelectronics due to its unique electronic properties. In this context, silicon carbide (SiC) surfaces have been proposed as ideal supports. Our study aims to evaluate the suitability of SiC coated with graphene for technological application, employing many-body perturbation theory to investigate the electronic structure and optical properties of graphene-covered 4H-SiC surfaces. Our analysis reveals that pristine 4H-SiC surfaces with dangling bonds exhibit a reduced transport gap and enhanced optically active states within the visible spectrum when compared to bulk 4H-SiC. The strong interfacial interactions resulting from the adsorption of a single graphene layer significantly alter graphene's dispersion, yielding a semiconducting interface with modified optoelectronic properties. While the addition of a second layer restores the Dirac dispersion, the two polar faces of the underlying 4H-SiC can induce either metallic n-type doping or behavior similar to freestanding graphene at the interface. Furthermore, We also investigate the adsorption of a molecular electron acceptor on SiC coated with one and two graphene layers. Our findings reveal notable renormalization of the molecular energy levels upon adsorption, leading to the formation of distinct new optically excited states. Additionally, we observe an upward shift in the Fermi level, suggesting partial surface charge transfer and effective p-type doping. The tunable doping characteristics and optical profiles across various energy ranges highlight the potential of graphene-covered 4H-SiC surfaces as versatile materials for a wide range of technological applications.

Introduction

Polytypes of SiC (silicon carbide) have garnered significant attention from the scientific community due to their unique properties and versatility. Among various intrinsic applications,[1] SiC surfaces have been proposed as ideal substrates for the growth of graphene layers (GLs).[2–13] Notably, the formation of GLs on different SiC polytype surfaces is highly dependent on the underlying crystal structure.[6,12] For instance, the epitaxial GLs on hexagonal polar,[7–11] nonpolar,[14,15] and cubic surfaces[16,17] exhibit notably different characteristics, caused by surface charge transfer.[3–5,7–11] Consequently, various configurations of GL/SiC interfaces have been proposed for vast numbers of technological applications.[6–11,13]

In this work, we focus on the hexagonal 4H-SiC surface with two polar faces: the C-terminated $(000\bar{1})$ and the Si-terminated (0001). These surfaces are commonly used in the fabrication of semiconductor devices and multi-layer heterostructures.[7–11] The growth of epitaxial GLs on these substrates begins with the formation of a buffer layer (BL), which is covalently bonded to the substrate and lacks the semi-metallic dispersion of freestanding graphene.[5,7,9,18,19] Nonetheless, subsequent GLs retain the pristine graphene features, though with different work functions, resulting in a metallic interface with n-type doped characteristics on the Si-terminated face and properties closer to freestanding graphene, including a semi-metallic zero-gap band structure, on the C-terminated face. In parallel with these experimental observations, standard density functional theory (DFT) has been widely used to identify the corresponding electron energy spectra and the nature of the interactions at the interface: strong interactions for the BL/SiC interface and weak van der Waals (vdW) interactions for the subsequent GLs.[9,12,20]

Considering the potential applications of graphene-covered SiC surfaces in optoelectronics, accurate descriptions of their electronic structure and optical absorption spectra are still relatively rare, with most studies focusing on bulk and clean surfaces of SiC polytypes.[21–24] Here, we employ many-body perturbation theory to thoroughly investigate the optoelectronic features of both polar faces of 4H-SiC, with and without GLs. Given the complex orbital-dependent properties of hexagonal SiC crystals,[22] it has been demonstrated that GW corrections[25] are crucial for achieving accurate quasiparticle results, thanks to the dynamical electronic correlation effects accounted for in the method.[26] Reliable optical absorption spectra can be obtained by applying quasiparticle corrections and incorporating bound excitonic effects in the electron-hole (e-h) coupling. To achieve the latter, we integrate our GW results with the solution of the Bethe-Salpeter equation (BSE).[26] This approach provides precise estimations of both charged and neutral excitations, required for the quantitative description of quasiparticle and absorption spectra, often showing excellent agreement with experimental results.[21,23,24,26,27] We also employ DFT and its time-dependent extension using the hybrid Heyd-Scuseria-Ernzerhof (HSE) functional, which incorporates screened Coulomb interactions and a fraction of exact exchange for short-range interactions.[28] Although the HSE functional provides a more accurate description of the electronic bandgap than purely (semi-)local functionals, it may suffer from deficiencies in describing long-range e-h interactions, thereby limiting its ability to characterize bound excitons accurately.[29–31] Despite this limitation, the HSE functional can still produce reasonable continuum spectra.[30]

Charge-transfer driven by molecular adsorption on free-standing graphene has been widely recognized as a promising method for compensating excess negative charges in epitaxial monolayers.[13,32,33] Likewise, molecular adsorption on the GL/SiC interfaces could potentially modify the electronic structure, offering valuable insights into the rearrangement of the electron density and possible interfacial charge transfer. Building on recent studies,[13,24] we investigate the adsorption of the electron-accepting molecule F6TCNNQ (2,2$'$-perfluoronaphthalene-2,6-diylidene dimalononitrile, also known as F6-TNAP[34]) on GL/SiC interfaces. Our focus is on the SiC(000$\bar{1}$) underlying surface, for which the formation of high-quality GLs with larger domain sizes and significantly improved charge carrier mobility has been observed.[7,11,24] As we demonstrate, a suitable bandgap size upon adsorption of the BL, and pristine-like (neutral) characteristic of the ensuing GLs, make the C-terminated substrate an excellent candidate to fine-tune the optoelectronic properties of GL/SiC interfaces through the adsorption of molecules whose substrate-dependent energy levels can introduce trap or recombination centers within the substrate.

This article begins with a brief review of the computational methods, followed by a comprehensive analysis of the quasiparticle and absorption spectra of the two polar faces of the clean 4H-SiC surface. Next, we evaluate the impact of adsorbing one and two GLs onto the 4H-SiC surfaces, highlighting key features in the band structures arising from interfacial interactions, charge transfer, and doping effects. Additionally, we illustrate how surface states and interface interactions modulate the optical properties. Finally, we discuss the adsorption of the F6TCNNQ molecule on the GL/SiC interfaces, demonstrating a significant renormalization of the adsorbate energy levels driven by the surface-induced screening. This renormalization leads to distinct optically excited states associated with the hybridization of molecular and substrate states, as well as *p*-type doping. The tunable *p*- or *n*-type doping characteristics of graphene-covered SiC surfaces make them highly versatile for advanced applications in optoelectronics and interface engineering.

Computational Details

Our primary substrate is hexagonal 4H-SiC, modeled using the experimental lattice constants as outlined in our previous study.[24] Experimentally, GLs grown on C-terminated 4H-SiC exhibit a complex periodicity of $\sqrt{3}\times\sqrt{3}$R30° (abbreviated as $\sqrt{3}$R),[8–10,35] while on the Si-terminated face, the larger $6\sqrt{3}\times6\sqrt{3}$R30° reconstruction covered by a 13×13 GL has been observed.[2,12] Although this latter configuration provides stress-free alignment at the Si-terminated interface, the large number of atoms in the primitive cell makes computational studies costly, even at the mean-field level.[36] To facilitate higher-level theoretical studies while keeping computations tractable, we employed the same $\sqrt{3}$R reconstruction commensurated with four graphene unit cells for both polar faces of the 4H-SiC surface, along with a vacuum interval of 14 Å, as shown in Supporting Information (SI) Figure S1. This simplified interface model, implying an elongation in the atop GL, is widely regarded as a practical approximation with no significant modification in the electronic structure compared to that of freestanding graphene.[9,12]

To investigate the adsorption of the F6TCNNQ acceptor, we focus on the C-terminated 4H-SiC covered by GL(s). Given the size of the F6TCNNQ molecule, our adsorption energy studies indicate that a 3×3 primitive cell of the $\sqrt{3}$R reconstruction is necessary to minimize interactions among periodic images of the adsorbate. Moreover, we previously demonstrated that the electronic structure exhibits only minor changes as the number of SiC bilayers varies.[24] Specifically, our detailed analysis at the DFT-HSE level, as shown in SI Figure S2, confirms minimal variations in bandgap and near-Fermi band structures for models with three and five SiC bilayers. Therefore, a 3×3 three-SiC-bilayer supercell model was used to mitigate the computational cost of molecular adsorption. It is worth noting that the Dirac cone of freestanding graphene appears at the Γ-point when their primitive cell is $3N \times 3N$ (N is an integer).[37,38]

The geometry optimization of all studied systems was carried out using spin-polarized DFT-HSE, as implemented in the VASP code.[39] We applied projector augmented wave potentials along with the Grimme-D3 correction[40] for vdW interactions. A plane wave cutoff energy of 400 eV and a Γ-centered 8×8×1 k-point grid were used, ensuring total energy convergence and interatomic forces were below 10^{-5} eV and 0.005 eV/Å, respectively. For substrates with the F6TCNNQ adsorbate, the HSE equilibrium geometry was obtained using single Γ-point sampling and a force convergence criterion of 0.01 eV/Å, while the actual HSE calculations were performed using a 2×2×1 k-point grid. All HSE band structures were explicitly computed along a specified k-path given by Ref.[41]

To compute the *GW* quasiparticle corrections, we used the perturbative one-shot G_0W_0 approach.[26] This involved constructing non-interacting Green's functions (G_0) based on mean-field Perdew-Burke-Ernzerhof (PBE) and HSE solutions, with the dynamical screened interaction (W_0) obtained at the random phase approximation (RPA) level. For pristine and GL-covered surfaces, G_0W_0 calculations were conducted using VASP with an $8 \times 8 \times 1$ mesh sampling and a total of 1240 bands, provided a convergence of 0.1 eV in the direct bandgaps. The electronic band structures along the specified k-path were obtained by interpolating the initial quasiparticle energies using localized Wannier functions.[42] Optical absorption and excitonic properties were subsequently calculated by solving the BSE within the Tamm-Dancoff approximation (TDA),[26] considering 12 bands on either side of the Fermi level. The same number of e-h states were used for solving the Casida equation[26] to obtain time-dependent DFT-HSE (TDHSE) spectra.

The *GW* calculations for the surface involving F6TCNNQ were performed using the BERKELEYGW package,[43] with DFT-PBE input provided by QUANTUM ESPRESSO.[44] Norm-conserving pseudo-potentials with a kinetic energy cutoff of 120 Ry were applied. The frequency dependence of the dielectric function was modeled using the plasmon-pole approximation,[26] with a $2 \times 2 \times 1$ sampling grid and a cutoff energy of 14 Ry. A total of 3000 bands were included, covering approximately 30 eV above the Fermi energy. The BSE-TDA spectrum was calculated using 14 occupied and 18 empty bands, with the BSE kernel interpolated to a finer Brillouin zone sampling of $8 \times 8 \times 1$.

The quasiparticle and optical properties of isolated F6TCNNQ were calculated using the all-electron MOLGW code[45] with a cc-pVQζ basis set. Given the lower computational cost in the gas phase, quasiparticle energies at the G_0W_0 level were computed using both semi-local and hybrid starting points. Additionally, the eigenvalue-only self-consistent GW (evGW) scheme was employed, with iterative corrections to the energies until the gap converged to within 0.01 eV. Note that the quasiparticle energies of the lowest unoccupied molecular orbital (LUMO) and highest occupied molecular orbital (HOMO) of an isolated molecule can be directly linked to the negative electron affinity (EA) and ionization energy (IE), respectively.[26,46] Optical absorption spectra, averaged over the three Cartesian components, were obtained by diagonalizing the BSE-TDA solutions.

Results & Discussion

Pristine 4H-SiC Surfaces

We begin our study by investigating the clean surfaces. The reconstructed 4H-SiC(000$\bar{1}$) surface, as illustrated in Figure 1a, was modeled with five SiC bilayers whose topmost layer consists of three C atoms, whereas the down-most Si atoms on the opposite side are H-passivated. HSE-relaxed geometry indicates that the unpaired C atoms in the topmost layer have a bond angle of 114° with the adjacent Si atoms, which is approximately 4% larger than the corresponding angles among Si-C-Si atoms in the lower layers. This increase results in a vertical distance of 0.42 Å (2.35 Å) between the topmost C layer and the lower Si (C) layer, which is 0.15 Å less than the distance in other layers. The other polar face, 4H-SiC(0001), was similarly modeled with five bilayers, with three unpaired Si atoms in the topmost layer and H-saturated carbon atoms in the opposite face. Equilibrium HSE geometry for this model reveals minor changes of approximately 1% in topmost C-Si-C bond angles, resulting in an almost negligible variation in the interlayer distances.

The three dangling bonds on the C-terminated face impose three singly occupied states

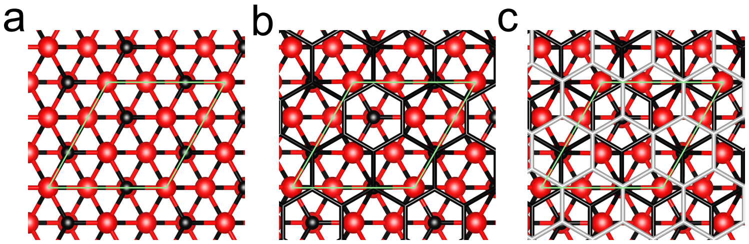

Figure 1: Top and side view of (a) the pristine 4H-SiC(000$\overline{1}$), (b) with the BL, and (c) the subsequent GL. The green hexagon outlines the $\sqrt{3}$R primitive cell. Red and black balls represent Si and C atoms. The black and silver sticks illustrate the BL and the subsequent GL, respectively.

(with a dominant role of $\mathrm{p_z}$ states) in the band structures, as depicted in Figure 2a by using three levels of theory. Compared to bulk 4H-SiC, which has an indirect gap of 3.29 eV and a direct gap of 4.56 eV (6.16 eV) at the M-point (Γ-point),[24] the presence of these in-gap states leads to notable changes in the electronic structure of the 4H-SiC(000$\overline{1}$) surface. The three theoretical approaches indicate the presence of a spin-down direct gap at the Γ-point, with values listed in Table 1. As previously suggested,[21] the semiconducting ground state points toward the occurrence of a Mott-Hubbard transition associated with a splitting corresponding to the on-site Coulomb repulsion energy. Our results similarly reveal a sizable splitting among the dangling-bond-induced states; while the HSE and G_0W_0@PBE methods suggest a mean splitting of 1.7 eV, the G_0W_0@HSE approach predicts a 0.5 eV larger value. Moreover, the dispersion of these in-gap states at the HSE level shows an increase of 0.5 eV (0.2 eV) for the occupied (empty) bands compared to those of the PBE. By applying the quasiparticle correction, this dispersion has been slightly increased, particularly for the empty states, for which appropriately accounting for the correlation energies is crucial.

For the reconstructed 4H-SiC(000$\overline{1}$) surface, the optical absorption spectra are shown in Figure 2b. Compared to bulk 4H-SiC, which exhibits an absorption onset in the ultraviolet (UV) region,[1,22–24] the C-terminated surface displays a pronounced red-shift and a broadened absorption spectrum that extends into the visible energy range. From a theoretical perspective, it is noteworthy that the optical structures predicted by TDHSE and BSE-G_0W_0@HSE are in close agreement. The BSE-G_0W_0@HSE calculations predict an absorption onset at

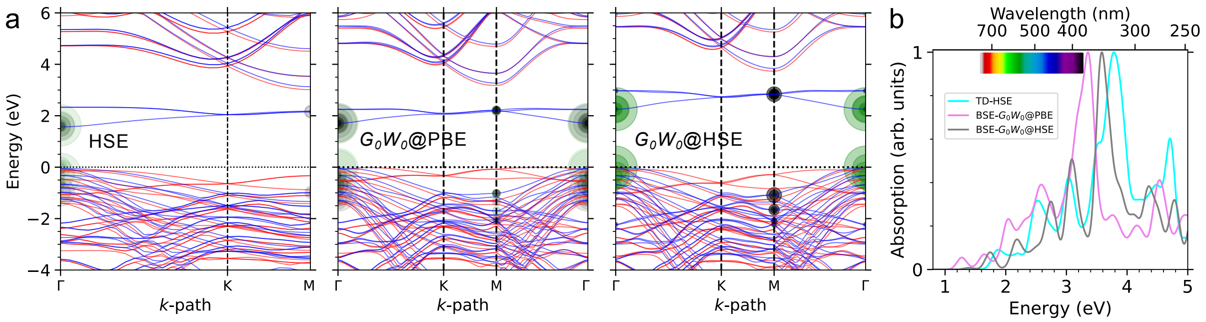

Figure 2: (a) The electronic band structures of 4H-SiC(000$\bar{1}$) obtained using three theoretical approaches. Spin majority and minority are represented in red and blue, respectively, with the VBM set to zero energy. (b) The corresponding optical absorption spectra, broadened using a Gaussian factor of 0.08 eV. The e-h eigenvalues involved in the excitations at the first two peaks are depicted by green and black circles, with magnified radii for clarity, representing the absolute value of the coupling coefficients.

1.39 eV, corresponding to a substantial exciton binding energy (ϵ_{b}) of 880 meV, followed by prominent peaks at 1.7, 2.2, 2.8, and 3.2 eV within the visible range. In comparison, TDHSE calculations estimate a slightly blue-shifted optical onset at 1.59 eV, reflecting a much smaller ϵ_{b} of 30 meV, with strong transitions at 1.8, 2.2, 2.6, and 3.1 eV. Both methods reveal qualitatively similar characteristics for these transitions. Specifically, for the two lowest-energy peaks, the e-h contributions with the largest coupling coefficients, illustrated by the circles in Figure 2a, predominantly reside in the spin-down channel and correspond to transitions from hole states at the bulk-like SiC valence edge to unoccupied in-gap surface states. The BSE-G_0W_0@PBE spectrum, while qualitatively similar to those obtained using TDHSE and BSE-G_0W_0@HSE, exhibits a significant red-shift, with the first two peaks appearing in the near-infrared (NIR) region. Despite this shift, the e-h contributions remain consistent with those identified in the other two approaches. Therefore, it implies that this red-shift arises directly from differences in quasiparticle bandgaps and points to the well-known starting-point dependency within the one-shot GW approach.[46]

Figure 3 presents the electronic structure and optical characteristics of the Si-terminated 4H-SiC(0001) surface, derived from the same three theoretical levels. The band structures indicate three singly occupied states resulting from the dangling bonds of the top Si atoms,

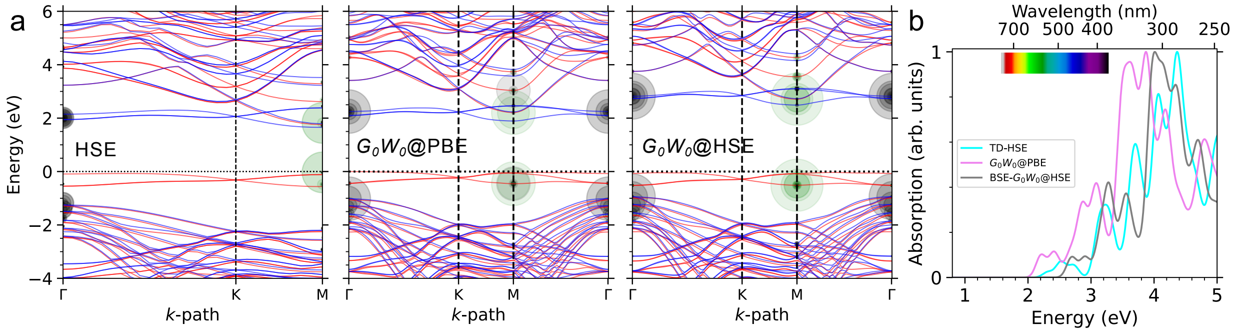

Figure 3: (a) The electronic band structures and (b) the optical absorption spectrum of 4H-SiC(0001) obtained using three different methods.

exhibiting a slightly larger splitting than seen in the C-terminated surface in Figure 2a. Furthermore, the occupied surface states in the Si-terminated surface demonstrate a separation of 0.5–0.7 eV from the bulk states, aligning with the photo-electron measurements.[12] This can be linked to the delocalization of Si dangling bonds and their higher energy compared to C atoms, which results in an upward shift of the Fermi energy and a reduced work function (see Table 1). Consequently, the band structures across the three theoretical levels indicate that the 4H-SiC(0001) surface possesses larger direct gaps than its C-face counterpart (see direct band gaps in Table 1). This difference contributes to a blue-shifted optical spectrum of 4H-SiC(0001), illustrated in Figure 3b. The e-h states related to the greenish onset and the first peak within the visible spectrum derive contributions from the band edges in both spin channels. The magnified green and black circles in the band structures highlight these contributions.

Graphene adlayer on the 4H-SiC surfaces

The most energetically stable stacking order of GL/4H-SiC(000$\bar{1}$) is illustrated in Figure 1b. At the interface, two carbon atoms of the surface are covalently bonded to the overlying GL, while the third atom, referred to as the C-deficient atom (C_D), is positioned below the hollow site of the graphene ring and remains with a dangling bond. The HSE geometry optimization indicates a bond length of 1.62 Å among bonded carbon atoms at the interface, in excellent

Table 1: Work functions (Φ) and direct bandgap energies at the Γ and M points, calculated for the majority (minority) spin channel using various theoretical approaches. The Φ values were obtained at the DFT-HSE level. All values are in eV.

	Φ	k-point	G_0W_0@PBE	HSE	G_0W_0@HSE
4H-SiC(000$\bar{1}$)	6.28	Γ	4.81 (1.68)	4.84 (1.62)	5.43 (2.27)
		M	3.21 (3.32)	3.34 (3.15)	4.02 (3.98)
BL/4H-SiC(000$\bar{1}$)	6.04	Γ	3.34 (2.57)	3.19 (2.71)	3.87 (3.19)
		M	2.64 (3.45)	2.73 (3.52)	3.22 (4.08)
4H-SiC(0001)	5.23	Γ	3.49 (3.12)	3.32 (3.20)	3.82 (3.68)
		M	2.26 (3.85)	1.87 (3.85)	2.79 (4.41)
BL/4H-SiC(0001)	3.56	Γ	——	0.42 (2.98)	1.09 (3.63)
		M	——	0.76 (2.86)	1.35 (3.46)

agreement with experimental measurements,[8] while the C_D atom relaxes outward. This results in a corrugation of 0.4 Å on either side of the interface, with a mean separation of 2.4 Å between the GL and the substrate. The stacking of the GL on the Si-terminated face follows a similar pattern: at the interface, the Si atom beneath the graphene hollow site, known as the lonely Si (Si_L), includes one unpaired electron per unit cell, while the other two Si atoms form direct bonds with graphene atoms, with a bond length of 2 Å, which is 6% longer than the corresponding bonds in the lower layers. Consequently, the equilibrium geometry shows a corrugation of 0.3 Å at the interface. The formation of covalent bonds at both C- and Si-terminated interfaces, combined with the distorted geometry, suppresses key features of free-standing graphene and causes the graphene adlayer to behave as a BL.[7,12,24]

Figure 4a shows the electronic band structure of 4H-SiC(000$\bar{1}$) covered by the BL obtained with three different methods. Notably, the presence of a singly occupied state, induced by the p_z state of the C_D atom, along with BL bands at the edges (see thicker lines in the HSE band structure), maintains the insulating phase of the substrate. Despite variations in bandgaps across different theoretical approaches, as listed in Table 1, we confirmed that the spatial distributions of the associated orbitals are comparable. For the C_D-induced state, moreover, all band structures reveal a strongly localized characteristic with a small dispersion of 0.1 eV and a mean splitting of 2, 2.5, and 2.9 eV at the G_0W_0@PBE, HSE,

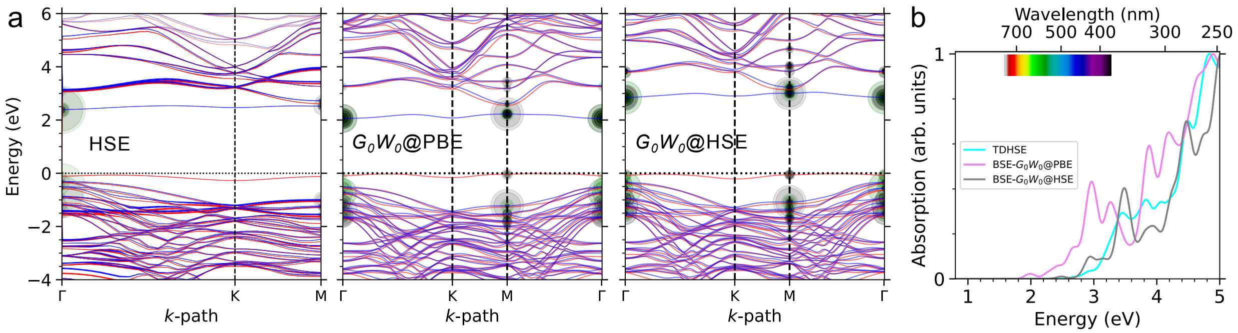

Figure 4: (a) The electronic structure and (b) optical properties of the BL/4H-SiC(000$\overline{1}$). In the HSE band structures, the contribution of the BL is highlighted with thicker lines. For the three optical absorption spectra, the e-h contributions involved in the excitations at the first and second peaks are represented by green and black circles, respectively, with magnified radii for clarity.

and G_0W_0@HSE levels, respectively. Compared to the clean surface in Figure 2, the smaller band dispersion of the $\mathrm{C_D}$-induced state can be attributed to the passivation effect imposed by the BL, which reduces the influence of the SiC substrate on the unbound atom, resulting in stronger localization of the state.

The optical absorption spectrum of the BL/4H-SiC(000$\overline{1}$) is shown in Figure 4b. All computed spectra exhibit a clear trace in the visible energy window. TDHSE and BSE-G_0W_0@HSE are in close agreement, suggesting two peaks at about 2.9 and 3.4 eV. Examining the involved e-h states, we found that these two excitations mainly stem from transitions between the spin-down valence bands and the unoccupied $\mathrm{C_D}$ state, as visualized by green and black circles on the band structures. The 3.4-eV transition additionally features some excitations with holes at the occupied $\mathrm{C_D}$ state. We should also note that the onset in TDHSE and BSE-G_0W_0@HSE spectra falls at 2.7 eV, showing the same origins as the 2.9 eV excitation but with holes confined in the Γ-point valence band maximum (VBM). The BSE-G_0W_0@PBE spectrum, on the other hand, qualitatively aligns with the two other spectra, with a systematic red-shift of 0.5 eV, linked mostly to gap differences, and shows the typical starting-point dependence of the G_0W_0 approximation.[26,46]

Now we focus on the electronic structure of the Si-terminated 4H-SiC surface covered

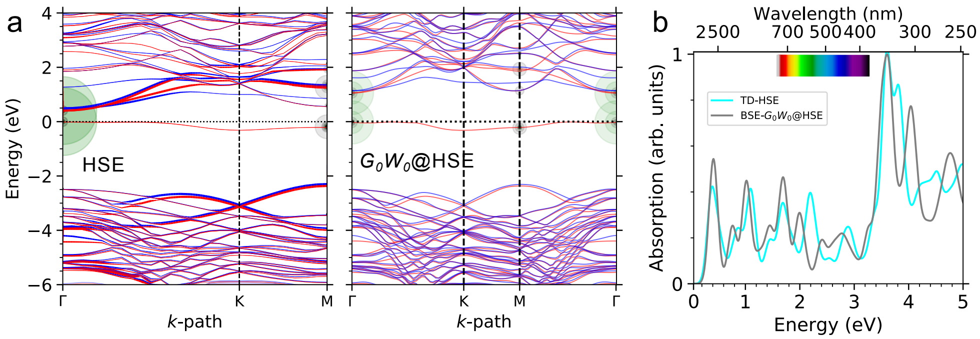

Figure 5: The electronic structure and optical properties of BL/4H-SiC(0001).

by a BL. Like previous calculations,[9] DFT-PBE calculations for this system predict a half-metallic ground state, with the upward-shifted Fermi level pinned by the $\mathrm{Si_L}$ state near the conduction band edge (see SI Figure S3). However, calculations using the hybrid HSE functional in Figure 5a reveal a semiconducting ground state with $\mathrm{Si_L}$ states being well-separated on either side of the bandgap (see bandgap values in Table 1). The discrepancy between the PBE and HSE predictions can be attributed to the limitations of the semilocal PBE functional, known to underestimate electronic correlations and misrepresent exchange interactions, particularly in systems with strong electronic localization or correlation effects. Thus, we place greater confidence in the HSE-derived semiconducting ground state, followed by the G_0W_0 quasiparticle corrections that further refine the energy levels and validate the gap characteristics.

Due to the delocalization of the Si surface states, as discussed for the corresponding clean surface, the dangling-bond-induced states exhibit greater dispersion with smaller splitting compared to the $\mathrm{C_D}$ state in Figure 4. This indeed indicates strong interactions at the interface between the Si-terminated face and the BL, leading to the charge transfer associated with an upward shift of the Fermi level, conferring n-type characteristics to the BL. Although the BL lacks the characteristic Dirac cone, a comparison of the bulk states in the band structures of the two polar faces in Figures 4 and 5 clearly shows the shift in Fermi energy (and the consequent impact on the work function) on the Si-terminated face compared to the C-terminated face. Furthermore, Bader charge analysis indicates that the BL on the

Si-terminated face gains an excess charge of 1.21 electrons, primarily accumulated on the atoms bonded to the two Si atoms at the interface, while the BL on the C-terminated face remains nearly neutral.

The optical absorption spectra are depicted in panel b of Figure 5. Similar to previous cases, there is a remarkable agreement between the TDHSE and BSE-G_0W_0@HSE spectra. Despite the differences in bandgap values estimated by HSE and G_0W_0@HSE, this consistency indicates the significant ϵ_b of 0.6 eV in the BSE solution. Consequently, the theoretical optical absorption spectrum of BL/4H-SiC(0001) spans a broad range, with a strong infrared onset at approximately 0.4 eV (3100 nm) and additional peaks at 0.76 and 1 eV. The e-h coupling coefficients of these excited states, represented by circles in the corresponding band structure, indicate transitions from the singly occupied $\mathrm{Si_L}$ state to the conduction band edge within the spin-majority channel. Importantly, the bulk-like hole states contribute dominantly to the absorption spectra at around 2.86 eV, closely resembling the absorption profile of the pristine surface.

BL/4H-SiC coated with an additional graphene layer

The adsorption of an additional GL in the Bernal configuration (the stacking pattern of graphite) is found to be the most energetically favorable arrangement.[3,9,12] Analyzing the HSE equilibrium geometry for both polar faces reveals that adding a second GL leads to negligible changes in the underlying structure. This is indeed consistent with the nearly planar structure of the second GL, which maintains a mean distance of 3.32 Å and 3.46 Å from the BL on Si- and C-terminated 4H-SiC, respectively. For comparison, the experimental value for the graphite interlayer distance (at room temperature) is determined to be 3.4 Å (3.6 Å).[3,36] As a result of the weak vdW bonding between the GL and the BL/4H-SiC, the characteristic graphene dispersion is expected to be preserved.

The HSE band structure of GL/BL/4H-SiC($000\bar{1}$) in Figure 6a confirms the appearance of the $\mathrm{C_D}$ states on either side of the Fermi level alongside the graphene-like dispersion.

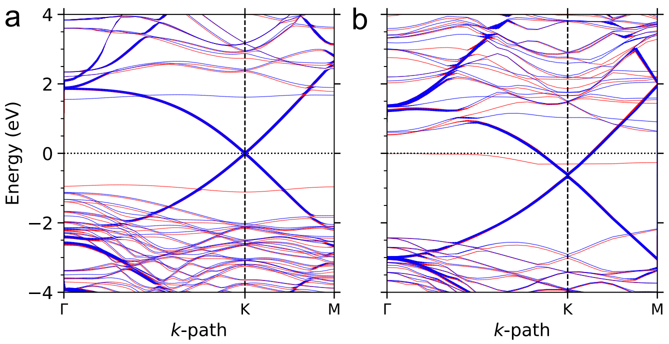

Figure 6: The HSE band structure of the (a) C-terminated and (b) Si-terminated faces of the $\sqrt{3}$R 4H-SiC covered by two GLs. Thicker lines highlight the contribution of the topmost GL.

Similar to freestanding graphene, the C_p orbitals in the topmost GL evolve into delocalized $\pi - \pi^*$ states at the band edges, resulting in the Dirac crossing-point and semi-metallic characteristics. It is also worth noting that the *GW* corrections applied on top of PBE and HSE yield a similar zero-gap band structure, as shown in SI Figure S4, with a more pronounced dispersive nature and slight variations in the C_D energies.

The adsorption of the subsequent GL on the BL/4H-SiC(0001), as shown in Figure 6b, also exhibits a graphene-like dispersion intersected by Si_L states. However, HSE calculations reveal a downward shift in the Fermi energy by 0.6 eV, indicating a pronounced *n*-type characteristic in the topmost GL. This result is consistent with recent UV-excited ARPES measurements,[13] which point to intrinsic *n*-type doping, with the Fermi energy positioned approximately 0.42 eV above the Dirac point. Applying Bader charge analysis, we found that the topmost GL accumulates an extra charge of 0.32 electrons, primarily on atoms positioned directly above the BL atoms. Compared to similar analysis for the BL/SiC system, this excess negative charge on the GL is donated from both the underlying BL and the Si_L atoms.

Adsorption of the F6TCNNQ on the graphene layer(s)/SiC interface

The adsorption of the F6TCNNQ acceptor was studied on 3×3 three-SiC-bilayer supercells covered by one and two GLs. For both substrates, the most stable adsorption site is achieved when the benzenoid rings of F6TCNNQ are positioned directly above the C–C bond of the lower GL, as detailed in SI Figure S5. In this configuration, the minimum distance between periodic images of the adsorbates exceeds 4 Å. In the HSE-optimized models, the adsorbate adopts an almost planar structure with slightly anchored cyano and fluorine ligands, maintaining an average separation of 3.3 Å from the lower GL/BL. This distance, comparable to the interlayer spacing in graphite, suggests similar weak vdW interactions between the substrate and the F6TCNNQ molecule.

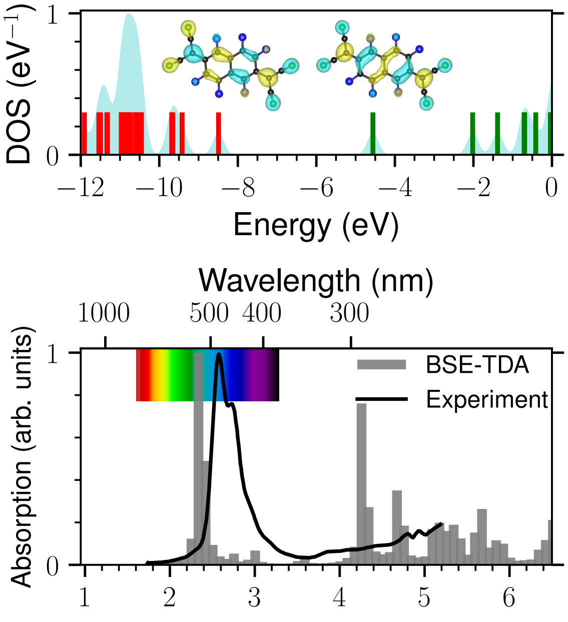

Figure 7: Quasiparticle energies obtained by G_0W_0@PBE and the corresponding optical absorption lines for the freestanding F6TCNNQ molecule. Occupied and unoccupied states are indicated by red and green vertical bars, respectively, and the spatial distributions of the HOMO and LUMO orbitals are illustrated. The experimental absorption spectrum, shown by the black solid curve, is adapted from Ref.[34]

Extracting the geometry of the F6TCNNQ molecule from the equilibrium models, we have computed the quasiparticle and adsorption spectra for the freestanding adsorbate, as shown in Figure 7. The G_0W_0@PBE quasiparticle spectrum indicates a gap of 3.93 eV (IE = 8.48 eV and EA = 4.55 eV) and the corresponding BSE-estimated absorption shows a strong excitation at 2.37 eV (ϵ_b=1.56) attributed to the dominant HOMO-to-LUMO transition. The latter agrees well with the given UV-visible spectrum[34] (solution absorbance in CH_2Cl_2), particularly for the first peak at 2.58 eV (481 nm). In SI Figure S6, we also gathered the quasiparticle and optical spectra obtained using hybrid starting points, as well as those obtained through the evGW scheme, which perfectly align with the available experimental data.

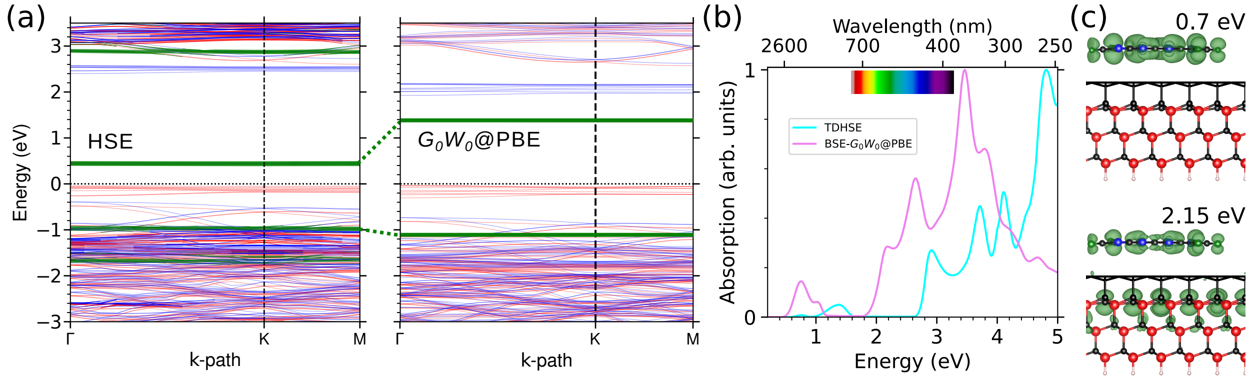

Figure 8: (a) Spin-polarized band structures and (b) the corresponding optical absorption spectra of F6TCNNQ on BL/4H-SiC $(000\bar{1})$. Projected bands onto the F6TCNNQ states are illustrated by green lines. (c) The spatial distribution of excitons corresponding to excitations at 0.7 eV and 2.15 eV in the BSE spectrum.

For F6TCNNQ on BL/4H-SiC$(000\bar{1})$, we computed the electronic structure and optical properties using two approaches, as illustrated in Figure 8. The HSE results reveal that the splitting and band dispersion of the localized C_D states are similar to those of the clean substrate, shown in Figure 4. By projecting the molecular states, we identified the localized LUMO of the adsorbate at 0.45 eV above the VBM, while the HOMO hybridizes with multiple states of BL/SiC, positioned approximately 1 eV below the VBM (see green lines in the band structure). Consequently, the HSE results indicate that the HOMO-LUMO gap of F6TCNNQ on the substrate is approximately 1.45 eV, which is close to that of the isolated molecule (see the HSE-DOS of the molecule in SI Figure S5). This surface-independent gap underscores the inability of the HSE functional to account for image charge effects and substrate-induced screening, which can significantly influence adsorbate energy levels.[47] To capture these effects, we performed G_0W_0@PBE calculations, as performing G_0W_0@HSE for such a large system is computationally prohibitive. The quasiparticle correction preserves a qualitatively similar electronic structure, with the splitting between $\mathrm{C_D}$ states being smaller than that obtained from HSE, yet still consistent with the results shown in Figures 2–4. However, upon inspecting the adsorbate's frontier orbitals in the quasiparticle band structure (Figure 8a), we find that the LUMO is located at 1.4 eV, while the HOMO is positioned at −1.1 eV. As a result, the quasiparticle HOMO-LUMO gap of the F6TCNNQ molecule adsorbed on BL/4H-SiC($000\overline{1}$) is 2.5 eV, significantly reduced compared to the quasiparticle HOMO-LUMO gap of the isolated molecule in Figure 7, which is 3.93 eV at the same level of theory. This substantial renormalization of the adsorbate gap highlights the critical role of substrate-induced screening effects, which are effectively captured by the GW approach.[24,47,48]

Compared to the absorption spectra of BL/4H-SiC($000\overline{1}$) shown in Figure 4, molecular adsorption on this surface introduces a new optical profile, as illustrated in Figure 8b. TDHSE reveals distinct excited states ranging from 1.3 to 1.7 eV (NIR region), with the involved e-h states indicating intermolecular transitions between the hybridized HOMO and the LUMO of the adsorbate. The G_0W_0-RPA (without e-h interactions) provides a qualitatively similar optical structure within the visible energy range, although with a noticeable blue shift (see SI Figure S8). This indeed confirms that the quality of near-edge orbitals, especially those influenced by the adsorbate, is comparable in both the PBE and HSE solutions.

Applying quasiparticle corrections and incorporating bound excitonic effects, the G_0W_0-BSE spectrum displays well-separated excitations at lower energies, with a main peak at 0.75 eV, showing a localized characteristic of the adsorbate LUMO when examining the corresponding exciton wavefunctions (see Figure 8c). Considering the quasiparticle adsorbate gap of 2.5 eV, therefore, the strong ϵ_b associated with this excitation suggests typical Frenkel-like intermolecular characteristics. Additionally, the BSE spectrum reveals three distinct peaks at 2.15, 2.65, and 3.45 eV. Given the similarity between these excitations and those on the clean BL/4H-SiC surface (see Figure 4), the enhanced intensities can be attributed to the contribution of the LUMO of the adsorbate. For example, the spatial distribution of the 2.15-eV exciton in Figure 8c highlights the combined contributions of the $\mathrm{C_D}$ electron states and the LUMO of the adsorbate.

Finally, we examine the qualitative effects of F6TCNNQ adsorption on the 4H-SiC(000$\overline{1}$) surface coated with two GLs. Given the metallic nature of this system at the mean-field level, an accurate quasiparticle description using semi-local PBE and hybrid HSE functionals would typically require a *GW* approach with at least partial self-consistency. However, due to the prohibitive computational demands of applying *GW* methods beyond the one-shot approach to such a large system, we limit our analysis to the DFT-HSE results. Nonetheless, the DFT-HSE approach, which incorporates a portion of the exact exchange, can model long-range interactions and hybridization in interfaces with complex vdW characteristics, offering a better representation of charge transfer compared to standard DFT, which tends to overestimate the degree of hybridization between the molecular orbitals and the substrate states (see DFT-PBE results in SI Figure S9).

The HSE band structure of the F6TCNNQ/GL/BL/SiC system is shown in Figure 9. While the graphene-like bands on either side of the Fermi energy intersect the $\mathrm{C_D}$ states with the same energy splitting as observed on the clean surface (see Figure 6), the projected states of the adsorbate similarly show surface-independent energy discretization. Upon F6TCNNQ adsorption, the most prominent feature is a 0.25 eV upward shift in the $\pi - \pi^*$ bands of the topmost GL, accompanied by a small splitting pinned by the LUMO of the adsorbate. This shift of the Dirac point above the Fermi level indicates p-type hybridization and partial charge transfer from the substrate to the adsorbate. The hybridization between the topmost

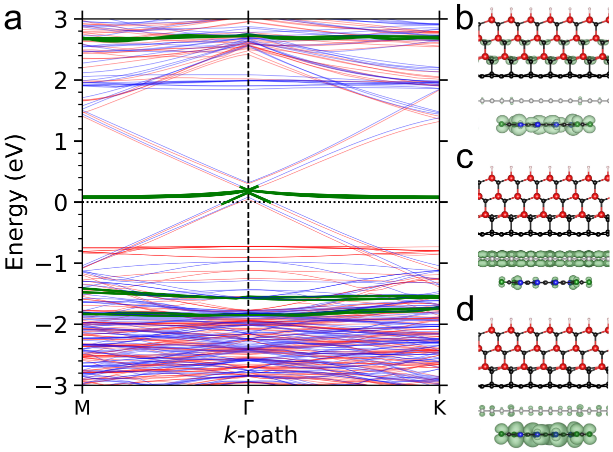

Figure 9: (a) The HSE band structure of F6TCNNQ on GL/BL/4H-SiC $(000\overline{1})$, with projected molecular states illustrated by green lines. The Fermi energy is set to zero. The isosurfaces of the HSE orbitals for (b) the adsorbate HOMO, (c) the graphene-π band, and (d) the adsorbate LUMO.

GL and the adsorbate is further illustrated by the spatial distribution of the GL_π state and the LUMO of the adsorbate, as shown in Figures 9c-d. Bader charge analysis supports this, revealing a partial charge transfer of 0.37 electrons from the substrate to the F6TCNNQ. Similar findings have been reported for F4TCNQ adsorbed on freestanding graphene, where partial charge transfer and a partially filled adsorbate LUMO results in an interface dipole, increasing the system's work function.[20,38,49]

Conclusion

We performed *GW* plus Bethe-Salpeter equation calculations for the two polar faces of 4H-SiC, coated with one and two graphene layers. For pristine surfaces, our results indicate that the semiconducting nature of the bulk is retained, albeit with a reduced fundamental gap, resulting in absorption spectra within the visible range. The adsorption of the first graphene layer, forming covalent bonds with the SiC substrate, induces a significant change in the electronic structure, with band gaps ranging from 1 eV on the Si-terminated face to 2.2 eV on the C-terminated face. This variation is attributed to differences in work function and stronger interfacial interactions on the Si-terminated face, leading to a broader optical absorption spectrum with an onset in the mid-infrared region. The adsorption of a second graphene layer restores the characteristic graphene dispersion. However, a downward shift in the Fermi level on the Si-terminated face indicates n-type doping, whereas the graphene layer adsorbed on the C-terminated face remains neutral, with the Fermi energy aligned at the Dirac point, exhibiting a semi-metallic nature.

For the C-terminated 4H-SiC coated with graphene layers, we also investigated the adsorption of the electron-accepting F6TCNNQ molecule. Our results show that the renormalized LUMO of the adsorbate, positioned within the bandgap of the substrate, leads to the emergence of new optically excited states. These excitations, well-separated from the surface states, offer desirable wavelength selectivity for optoelectronic applications. Additionally, molecular adsorption on SiC($000\bar{1}$) coated with two graphene layers clearly demonstrates p-type doping at the interface, resulting from partial charge transfer from the substrate to the adsorbate.

From a theoretical perspective, our findings on the optical properties of SiC and Gr/SiC systems show close agreement between the TDHSE and BSE-G_0W_0@HSE results. For molecular adsorption, however, employing a GW scheme is crucial for accurately capturing the effects of surface screening on the energy levels of the adsorbate.

In conclusion, our comprehensive theoretical study highlights the potential of graphene/SiC interfaces for effectively modulating optoelectronic properties. Additionally, the fine-tuned p- and n-type doping mechanisms at these interfaces offer precise control for various technological applications.

Supporting Information Available

The Supporting Information is available free of charge at https://pubs.acs.org/doi/

- Additional details on convergence tests, the electronic structure at mean-field levels, geometry optimization, and isolated molecule spectra (PDF).

Acknowledgement

All calculations were performed at the Mare Nostrum Supercomputer of the Red Española de Supercomputación (BSC-RES) and the Centro de Computación Científica de la Universidad Autónoma de Madrid (CCC-UAM). This work has been supported by the European Research Council (ERC) under the European Unions Horizon 2020 research and innovation programme (grant agreement no. 951224, TOMATTO), the Ministerio de Ciencia e Innovación MICINN (Spain) through the projects PID2022-138288NB-C31 and PID2022-138288NB-C33, the "Severo Ochoa" Programme for Centres of Excellence in R&D (CEX2020-001039-S), and the "María de Maeztu" Programme for Units of Excellence in R&D (CEX2018-000805-M).

References

(1) Levinshtein, M. E.; Rumyantsev, S. L.; Shur, M. S. *Properties of Advanced Semiconductor Materials: GaN, AIN, InN, BN, SiC, SiGe*; John Wiley & Sons, 2001.

(2) Zhao, J.; Ji, P.; Li, Y.; Li, R.; Zhang, K.; Tian, H.; Yu, K.; Bian, B.; Hao, L.; Xiao, X. et al. Ultra-high mobility semiconducting epitaxial graphene on silicon carbide. *Nature* **2024**, *625*, 60–65.

(3) Ohta, T.; Bostwick, A.; Seyller, T.; Horn, K.; Rotenberg, E. Controlling the Electronic Structure of Bilayer Graphene. *Science* **2006**, *313*, 951–954.

(4) Ohta, T.; Bostwick, A.; McChesney, J. L.; Seyller, T.; Horn, K.; Rotenberg, E. Interlayer Interaction and Electronic Screening in Multilayer Graphene Investigated with Angle-Resolved Photoemission Spectroscopy. *Phys. Rev. Lett.* **2007**, *98*, 206802.

(5) Zhou, S. Y.; Gweon, G. H.; Fedorov, A. V.; First, P. N.; de Heer, W. A.; Lee, D. H.; Guinea, F.; Castro Neto, A. H.; Lanzara, A. Substrate-induced bandgap opening in epitaxial graphene. *Nature Mater.* **2007**, *6*, 770.

(6) Giannazzo, F. Insight into the mechanisms of chemical doping of graphene on silicon carbide. *Nanotechnology* **2016**, *27*, 072502.

(7) Hass, J.; Feng, R.; Li, T.; Li, X.; Zong, Z.; de Heer, W. A.; First, P. N.; Conrad, E. H.; Jeffrey, C. A.; Berger, C. Highly ordered graphene for two dimensional electronics. *Appl. Phys. Lett.* **2006**, *89*, 143106.

(8) Hass, J.; Feng, R.; Millán-Otoya, J. E.; Li, X.; Sprinkle, M.; First, P. N.; de Heer, W. A.; Conrad, E. H.; Berger, C. Structural properties of the multilayer graphene/$4H-$SiC$(000\bar{1})$ system as determined by surface x-ray diffraction. *Phys. Rev. B* **2007**, *75*, 214109.

(9) Varchon, F.; Feng, R.; Hass, J.; Li, X.; Nguyen, B. N.; Naud, C.; Mallet, P.; Veuillen, J.-Y.; Berger, C.; Conrad, E. H. et al. Electronic Structure of Epitaxial Graphene Layers on SiC: Effect of the Substrate. *Phys. Rev. Lett.* **2007**, *99*, 126805.

(10) Forbeaux, I.; Themlin, J.-M.; Debever, J.-M. High-temperature graphitization of the 6H-SiC (0001) face. *Surf. Sci.* **1999**, *442*, 9–18.

(11) Berger, C.; Song, Z.; Li, X.; Wu, X.; Brown, N.; Naud, C.; Mayou, D.; Tianbo, L.; Hass, J.; Marchenkov, A. M. et al. Electronic Confinement and Coherence in Papperned Epitaxial Graphene. *Science* **2006**, *312*, 1191–1196.

(12) Mattausch, A.; Pankratov, O. Density functional study of graphene overlayers on SiC. *Phys. Status Solidi b* **2008**, *245*, 1425–1435.

(13) Coletti, C.; Riedl, C.; Lee, D. S.; Krauss, B.; Patthey, L.; von Klitzing, K.; Smet, J. H.;

Starke, U. Charge neutrality and band-gap tuning of epitaxial graphene on SiC by molecular doping. *Phys. Rev. B* **2010**, *81*, 235401.

(14) Ostler, M.; Deretzis, I.; Mammadov, S.; Giannazzo, F.; Nicotra, G.; Spinella, C.; Seyller, T.; La Magna, A. Direct growth of quasi-free-standing epitaxial graphene on nonpolar SiC surfaces. *Phys. Rev. B* **2013**, *88*, 085408.

(15) Daas, B. K.; Omar, S. U.; Shetu, S.; Daniels, K. M.; Ma, S.; Sudarshan, T. S.; Chandrashekhar, M. V. S. Comparison of Epitaxial Graphene Growth on Polar and Nonpolar 6H-SiC Faces: On the Growth of Multilayer Films. *Cryst. Growth Des.* **2012**, *12*, 3379–3387.

(16) Ouerghi, A.; Marangolo, M.; Belkhou, R.; El Moussaoui, S.; Silly, M. G.; Eddrief, M.; Largeau, L.; Portail, M.; Fain, B.; Sirotti, F. Epitaxial graphene on 3C-SiC(111) pseudosubstrate: Structural and electronic properties. *Phys. Rev. B* **2010**, *82*, 125445.

(17) Darakchieva, V.; Boosalis, A.; Zakharov, A. A.; Hofmann, T.; Schubert, M.; Tiwald, T. E.; Iakimov, T.; Vasiliauskas, R.; Yakimova, R. Large-area microfocal spectroscopic ellipsometry mapping of thickness and electronic properties of epitaxial graphene on Si- and C-face of 3C-SiC(111). *Appl. Phys. Lett.* **2013**, *102*, 213116.

(18) Hass, J.; de Heer, W. A.; Conrad, E. H. The growth and morphology of epitaxial multilayer graphene. *J. Condens. Matter Phys.* **2008**, *20*, 323202.

(19) Ruan, M.; Hu, Y.; Guo, Z.; Dong, R.; Palmer, J.; Hankinson, J.; Berger, C.; de Heer, W. A. Epitaxial graphene on silicon carbide: Introduction to structured graphene. *MRS Bulletin* **2012**, *37*, 11381147.

(20) Chi, M.; Zhao, Y.-P. First principle study of the interaction and charge transfer between graphene and organic molecules. *Comput. Mater. Sci.* **2012**, *56*, 79–84.

(21) Rohlfing, M.; Pollmann, J. Parameter of the Mott-Hubbard Insulator 6HSiC(0001) $\sqrt{3} \times \sqrt{3}R30^\circ$: An Ab Initio Calculation. *Phys. Rev. Lett.* **2000**, *84*, 135–138.

(22) Cannuccia, E.; Gali, A. Thermal evolution of silicon carbide electronic bands. *Phys. Rev. Mater.* **2020**, *4*, 014601.

(23) Zhang, X.; Kioupakis, E. Phonon-assisted optical absorption of SiC polytypes from first principles. *Phys. Rev. B* **2023**, *107*, 115207.

(24) Mansouri, M.; Díaz, C.; Martín, F. Optoelectronic properties of electron-acceptor molecules adsorbed on Graphene/Silicon Carbide interfaces. *Commun. Mater.* **2024**, *5*, 117.

(25) Hedin, L. New Method for Calculating the One-Particle Green's Function with Application to the Electron-Gas Problem. *Phys. Rev.* **1965**, *139*, A796–A823.

(26) Martin, R. M., Reining, L., Ceperley, D. M., Eds. *Interacting Electrons: Theory and Computational Approaches*; Cambridge University Press, 2016.

(27) Mansouri, M.; Koval, P.; Sharifzadeh, S.; Snchez-Portal, D. Molecular Doping in the Organic Semiconductor Diindenoperylene: Insights from Many-Body Perturbation Theory. *J. Phys. Chem. C* **2023**, *127*, 16668–16678.

(28) Heyd, J.; Scuseria, G. E.; Ernzerhof, M. Hybrid functionals based on a screened Coulomb potential. *J. Chem. Phys.* **2003**, *118*, 8207–8215.

(29) Paier, J.; Marsman, M.; Kresse, G. Dielectric properties and excitons for extended systems from hybrid functionals. *Phys. Rev. B* **2008**, *78*, 121201.

(30) Yang, Z.-h.; Sottile, F.; Ullrich, C. A. Simple screened exact-exchange approach for excitonic properties in solids. *Phys. Rev. B* **2015**, *92*, 035202.

(31) Mansouri, M.; Lewis, D. K.; Sharifzadeh, S. Introduction of localized spin-state transitions in the optical absorption spectrum of Cr-doped GaN. *Phys. Rev. B* **2023**, *107*, 184103.

(32) Otero, R.; Miranda, R.; Gallego, J. M. A Comparative Computational Study of the Adsorption of TCNQ and F4-TCNQ on the Coinage Metal Surfaces. *ACS Omega* **2019**, *4*, 16906–16915.

(33) de Oliveira, I. S. S.; Miwa, R. H. Organic molecules deposited on graphene: A computational investigation of self-assembly and electronic structure. *J. Chem. Phys.* **2015**, *142*, 044301.

(34) Koech, P. K.; Padmaperuma, A. B.; Wang, L.; Swensen, J. S.; Polikarpov, E.; Darsell, J. T.; Rainbolt, J. E.; Gaspar, D. J. Synthesis and Application of 1,3,4,5,7,8 - Hexafluoro tetracyanonaphthoquinodimethane (F6-TNAP): A Conductivity Dopant for Organic Light-Emitting Devices. *Chem. Mater.* **2010**, *22*, 3926–3932.

(35) Berger, C.; Song, Z.; Li, X.; Wu, X.; Brown, N.; Naud, C.; Mayou, D.; Li, T.; Hass, J.; Marchenkov, A. N. et al. Electronic Confinement and Coherence in Patterned Epitaxial Graphene. *Science* **2006**, *312*, 1191–1196.

(36) Cavallucci, T.; Tozzini, V. Multistable Rippling of Graphene on SiC: A Density Functional Theory Study. *J. Phys. Chem. C* **2016**, *120*, 7670–7677.

(37) Zhou, Y.-C.; Zhang, H.-L.; Deng, W.-Q. A 3N rule for the electronic properties of doped graphene. *Nanotechnology* **2013**, *24*, 225705.

(38) Pinto, H.; Jones, R.; Goss, J. P.; Briddon, P. R. p-type doping of graphene with F4-TCNQ. *J. Condens. Matter Phys.* **2009**, *21*, 402001.

(39) Kresse, G.; Furthmüller, J. Efficient iterative schemes for ab initio total-energy calculations using a plane-wave basis set. *Phys. Rev. B* **1996**, *54*, 11169–11186.

(40) Grimme, S. Semiempirical GGA-type density functional constructed with a long-range dispersion correction. *J. Comput. Chem.* **2006**, *27*, 1787–1799.

(41) Wang, V.; Xu, N.; Liu, J.-C.; Tang, G.; Geng, W.-T. VASPKIT: A user-friendly interface facilitating high-throughput computing and analysis using VASP code. *Comput. Phys. Commun.* **2021**, *267*, 108033.

(42) Pizzi, G.; Vitale, V.; Arita, R.; Blgel, S.; Freimuth, F.; Granton, G.; Gibertini, M.; Gresch, D.; Johnson, C.; Koretsune, T. et al. Wannier90 as a community code: new features and applications. *J. Phys. Condens.* **2020**, *32*, 165902.

(43) Deslippe, J.; Samsonidze, G.; Strubbe, D. A.; Jain, M.; Cohen, M. L.; Louie, S. G. BerkeleyGW: A massively parallel computer package for the calculation of the quasiparticle and optical properties of materials and nanostructures. *Comput. Phys. Commun.* **2012**, *183*, 1269–1289.

(44) Giannozzi, P.; Baroni, S.; Bonini, N.; Calandra, M.; Car, R.; Cavazzoni, C.; Ceresoli, D.; Chiarotti, G. L.; Cococcioni, M.; Dabo, I. et al. QUANTUM ESPRESSO: a modular and open-source software project for quantum simulations of materials. *J. Phys. Condens. Matter* **2009**, *21*, 395502.

(45) Bruneval, F.; Rangel, T.; Hamed, S. M.; Shao, M.; Yang, C.; Neaton, J. B. MOLGW 1: Many-body perturbation theory software for atoms, molecules, and clusters. *Comput. Phys. Commun* **2016**, *208*, 149–161.

(46) Mansouri, M.; Casanova, D.; Koval, P.; Sánchez-Portal, D. *GW* approximation for open-shell molecules: a first-principles study. *New J. Phys.* **2021**, *23*, 093027.

(47) Garcia-Lastra, J. M.; Rostgaard, C.; Rubio, A.; Thygesen, K. S. Polarization-induced renormalization of molecular levels at metallic and semiconducting surfaces. *Phys. Rev. B* **2009**, *80*, 245427.

(48) Neaton, J. B.; Hybertsen, M. S.; Louie, S. G. Renormalization of Molecular Electronic Levels at Metal-Molecule Interfaces. *Phys. Rev. Lett.* **2006**, *97*, 216405.

(49) Chen, W.; Chen, S.; Qi, D. C.; Gao, X. Y.; Wee, A. T. S. Surface Transfer p-Type Doping of Epitaxial Graphene. *J. Am. Chem. Soc.* **2007**, *129*, 10418–10422.

TOC Graphic